Calculation of the phase diagram of ^{3}He-^{4}He solid and liquid mixtures

D. O. Edwards* and S. Balibar

Groupe de Physique des Solides de l'Ecole Normale Supérieure, 24 rue Lhomond, 75231 Paris CEDEX 05, France
(Received 6 June 1988)

The phase diagram of ^{3}He-^{4}He mixtures has been calculated for temperatures from ~ 0.02 to ~ 1 K using well-known phenomenological models to describe the liquid and crystalline phases. For the bcc and hcp phases the regular solution model is shown to agree with measurements of the isotopic phase separation and the hcp-bcc transformation. The theory can be applied in thermodynamic equilibrium or when the crystalline transformation is too slow for complete equilibrium to be reached. For the liquid phases the theory is confined to fairly dilute solutions of either ^{3}He or ^{4}He, where the models of Landau and Pomeranchuk and Zharkov and Silin can be applied. The input parameters for the calculation are taken mostly from measurements made on the pure isotopes or single-phase mixtures. The analysis includes the determination of the free-energy difference at $T=0$ between the bcc and hcp structures in both pure ^{4}He and pure ^{3}He. The calculated phase diagram agrees well with experiment, mostly within the experimental uncertainties which are sometimes quite large. The comparison with experiment includes measurements of freezing and melting curves, univariants (three-phase equilibrium lines) and the two quadruple points. Parts of the phase diagram which have not yet been measured are described in detail.

I. INTRODUCTION

This paper deals with the phase diagram of liquid and solid ^{3}He-^{4}He mixtures primarily in the temperature range from about 0.02 to 0.5 K. These temperatures are such that, in the crystalline phases, ordering of the ^{3}He nuclear spins and the effect of thermally excited phonons are both almost negligible. At the same time, in the liquid phases, we are well below the superfluid transition in the ^{4}He-rich liquid and well above it in the ^{3}He-rich liquid. Even so, the phase diagram is well known[1,2] to be very complicated, with two, or possibly three,[3] quadruple points: points in the pressure-temperature (PT) plane where four phases may coexist. The complexity is due to phase separation of the isotopes in both the liquid and the solid, and to the existence of two crystalline structures in the solid at low pressure, hexagonal close packed (hcp) and body-centered cubic (bcc).

The work we describe is a calculation of the phase diagram using well-known phenomenological models to describe each of the liquid and crystalline phases. Such a calculation, which has not been performed before, is useful in several ways: First, it allows the extensive measurements on the phase diagram to be used to test the accuracy of these models and to determine some of the empirical parameters contained in them. For instance, by applying the "regular solution model" to solid mixtures of ^{3}He and ^{4}He, we have found that it provides a fairly accurate description of both the isotopic phase separation and the crystalline hcp-bcc transformation. This is one of the principal results in the paper. Secondly, a theoretical description of the phase diagram allows one to make predictions for regions of the P-T-X space (X is the ^{3}He concentration) where measurements have not yet been made. For example, ^{3}He bcc crystals at low temperatures have recently been observed[4] to grow dendritically when small amounts of ^{4}He are present. To interpret these measurements, the relative solubility of ^{4}He in bcc and in liquid ^{3}He must be known as a function of concentration and temperature. A formula for this is given at the end of the paper. (In general, a calculation of any part of the phase diagram requires a simple computer calculation as described in the Appendix.) A third application of the theory is that it suggests experiments which are not direct measurements of the phase diagram but which cast light on its structure. Since direct measurements are often hampered by very long relaxation times, superheating and supercooling etc., these experiments can be more accurate and easier to carry out than direct measurements.

The paper is written in the following order: Section II is on the regular solution model and its application to solid ^{3}He-^{4}He mixtures; Sec. III deals with the determination of the free-energy difference between hcp and bcc ^{3}He or ^{4}He, and the fit of the regular solution model to various experiments; Sec. IV is on models appropriate for liquid mixtures and their application to complete the calculation of the phase diagram; and Sec. V contains our conclusions.

In comparing the theory with experiments on solid mixtures, we may allow for the fact that equilibrium with respect to the crystal structure is attained much more slowly than for the separation of the isotopes, so that sometimes only partial equilibrium is attained. How this is done is explained in Sec. II C.

In Sec. III E we include the effects of thermal phonons using a simple approximation. This allows the theory to be extended up to ~ 1 K or more, provided the concentration of either ^{3}He or ^{4}He is not too large. The phonon terms have been included in all the numerical calculations described in the paper, but their effect is negligible below ~ 0.5 K.

II. ISOTOPIC PHASE SEPARATION AND THE bcc-hcp TRANSFORMATION IN SOLID ^{3}He-^{4}He

A. The regular solution model

The regular solution model relates the Gibbs free energy $g(P,T,X)$ of a mixture of ^{3}He concentration X to the Gibbs energies of the pure substances g_3 and g_4. We define the "excess" free-energy g_E per atom by the equation

$$g(P,T,X) = (1-X)g_4(P,T) + Xg_3(P,T)$$
$$- TS_m(X) + g_E(P,T,X) , \qquad (1)$$

where

$$S_m = -k_B[X \ln X + (1-X)\ln(1-X)] \qquad (2)$$

is the classical entropy of mixing. In a regular solution g_E has a particular, simple form[5]

$$g_E = AX(1-X) , \qquad (3)$$

where the quantity A depends only on the pressure P. Since g, as defined by (1) to (3), is a continuous function of X, from $X = 0$ to 1, the model cannot be applied directly to situations where the pure states have different crystal symmetry. On the other hand, we can apply it separately to the two structures hcp and bcc, with two different constants A^h and A^b to interpolate between states of the pure isotopes with the same structure. Defining the free-energy differences,

$$\Delta_4(P,T) = g_4^b(P,T) - g_4^h(P,T) ,$$
$$\Delta_3(P,T) = g_3^h(P,T) - g_3^b(P,T) , \qquad (4)$$

between the metastable and the stable pure phases, then the excess free energy defined with respect to hcp ^{4}He and bcc ^{3}He, is

$$g_E^h = A^h X(1-X) + X\Delta_3 \qquad (5)$$

for a mixture which has the hexagonal structure, and

$$g_E^b = A^b X(1-X) + (1-X)\Delta_4 \qquad (6)$$

for a bcc mixture.

The regular solution model Eqs. (1) to (3), without taking differences in structure into account, fit the phase separation data of Edwards, McWilliams, and Daunt[6] (EMD) quite closely. The model gives, below a critical temperature $T_c = A/2k_B$, separation into two phases of concentrations X and $1-X$ where the temperature and concentration are related by

$$k_B T = A(1-2X)/\ln(X^{-1}-1) . \qquad (7)$$

The phase-separation line, shown in Fig. 1, is symmetrical about $X = \frac{1}{2}$.

The specific heat of the phase-separated mixture, measured in the EMD experiment, is

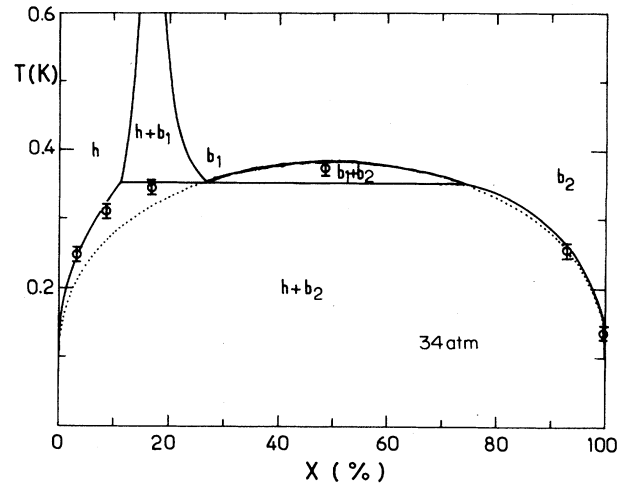$$C/k_B = \frac{(1-2X)^2}{\tau\left[\dfrac{\tau}{4X(1-X)} - 1\right]} , \qquad (8)$$

FIG. 1. The equilibrium phase diagram for hcp and bcc helium at $P = 34$ atm, assuming that hcp and bcc mixtures are regular. The hcp, bcc$_1$, and bcc$_2$ phases are labeled h, b_1, and b_2. The b_1-b_2 equilibrium line is given by Eq. (7). It has been extended (dotted line) into the $(h+b_2)$ region for comparison with the h-b_2 equilibrium lines. (Note the asymmetry of the h-b_1 and h-b_2 parts of the diagram.) The horizontal line represents the temperature at which the three phases h, b_1, and b_2 may be in equilibrium. In P-T-X space, such lines form a ruled surface called a univariant. The experimental points are from Ref. 7. Although the agreement with the theory is fairly good, the measurements did not achieve equilibrium with respect to the hcp-bcc transformation.

where X is a function of T, given by (7), and $\tau = T/T_c = 2k_B T/A$. This means that the specific heat below the phase-separation (PS) temperature,

$$T_{PS}(X_0) = (A/k_B)(1-2X_0)/\ln(X_0^{-1}-1) ,$$

does not depend on the initial concentration of the sample X_0, but follows a universal curve.

In writing (8), we have neglected the small lattice specific heat and the equally negligible nuclear-spin specific heat. We make this approximation in most of the paper. It means that, in the temperature range (0.02 to 0.5 K), g_4 depends solely on the pressure while the temperature dependence of g_3 is $g_3(P,T) = g_3(P,0) - k_B T \ln 2$.

The empirical value of A/k_B, fitted to the data of EMD at 35.8 atm, is 0.76 K. This value and its pressure dependence, the volume $B = dA/dP$, measured by Panczyk et al.[7] and others, are explained by theories developed by Prigogine and his collaborators,[8] Klemens et al.,[9] Coldwell-Horsfall,[10] and Mullin.[11] The two main results of the theories are the following: First that the isotopes are randomly arranged in the crystal lattice, in agreement with the classical mixing entropy, Eq. (2). Second that the energy change in mixing the pure isotopes is mostly the work done in compressing the ^{3}He and expanding the ^{4}He, so as to bring the two crystals to the same lattice spacing. The theories neglect differences in crystal structure, but give values for A which agree

with experiment quite well.

One difficulty in obtaining a precise value of A from these theories is that one needs the properties of pure crystalline ^{4}He where, in fact, the liquid is stable. Moreover, Mullin predicted that the simple quadratic dependence of g_E on X in Eq. (3) is only an approximation, and that there should be an asymmetry in the phase-separation curve. Such an asymmetry was apparently observed in the constant-volume pressure measurements of Panczyk, Scribner, Gonano, and Adams[7] (PSGA).

One way to represent such an asymmetry in the excess free energy is to modify (3) to

$$g_E = AX(1-X)(1+\epsilon X) , \qquad (9)$$

where the quantity ϵ is approximately -0.1, according to Mullin's calculations and the measurements of PSGA. (An even larger value, ~ -0.2, was recently proposed by Uwaha and Baym,[12] based on a particular analysis of some of the x-ray data of Fraass and Simmons.[13] A more general analysis,[14] based on all of the data, does not seem to confirm this result.)

With the asymmetry included, the equations for the phase-separation curve, the pressure at constant volume and the specific heat, which are derived from the equality of the ^{3}He and ^{4}He chemical potentials μ_3 and μ_4 between the two phases, are much more complicated and we have solved them numerically. In comparing the theory with the EMD experiment, we have taken into account the small change in pressure during the measurements of the specific heat which were performed at constant volume. We find that the specific heat, which no longer follows a universal curve, does not agree with the results of EMD if ϵ is assumed to be -0.1. Consistency with the EMD data requires that $\epsilon = 0 \pm 0.006$.

This conclusion is in agreement with the recent results of Ehrlich and Simmons[15,16] who concluded that $\epsilon = 0 \pm 0.01$. Ehrlich and Simmons used x-ray measurements of T_{PS} on a series of bcc single crystals with concentrations from $X_0 = 10\%$ to 70%. In contrast with PSGA, T_{PS} was determined when the crystal was first cooled into the phase-separation region.

In what follows we shall demonstrate that the large asymmetry observed by PSGA was probably caused by the effects of the bcc-hcp transition. Since the asymmetry ϵ from EMD and Ehrlich and Simmons is so small we shall henceforth neglect it.

The excellent agreement between the specific heat data of EMD and the simple regular solution model (with $\epsilon = 0$) demonstrates that the solid samples in their experiments, which were initially bcc, separated into two bcc phases. Apparently the bcc-hcp transformation in the ^{4}He-rich phase did not take place. Such a metastability of the bcc ^{4}He-rich phase is consistent with other experiments we have analyzed, for example that of Iwasa and Suzuki.[17] However, in the PSGA experiment, the crystalline transformation was observed to take place very slowly at all temperatures below the phase-separation temperature T_{PS}.

B. Regular solution bcc-hcp phase diagram

The chemical potentials in a bcc or hcp mixture, $\mu_3 = g + (1-X)(\partial g/\partial X)$ and $\mu_4 = g - X(\partial g/\partial X)$ from (5) and (6) substituted in (1) and (2), are

$$\begin{aligned} \mu_3^{b(h)} &= g_3^b + A^{b(h)}(1-X)^2 + k_B T \ln X \quad (+\Delta_3) , \\ \mu_4^{h(b)} &= g_4^h + A^{h(b)}X^2 + k_B T \ln(1-X) \quad (+\Delta_4) , \end{aligned} \qquad (10)$$

where the term in Δ_3 appears only in μ_3^h, and that in Δ_4 only in μ_4^b.

The phase diagram resulting from equating μ_3 and μ_4 between phases in equilibrium at a pressure of 34 atm is shown in Fig. 1. The choice of the parameters A^b, A^h, Δ_3, and Δ_4 used in calculating this diagram is explained in Sec. III.

In Fig. 1, at the triple point temperature $T_{tr}(P) = 0.353$ K, equilibrium between three phases, hcp, bcc$_1$, and bcc$_2$, is possible. (In common with other authors we use the subscripts 1 and 2 to denote the ^{4}He-rich and ^{3}He-rich phases.) The coexistence of three phases represents a univariant state where, following the phase rule, there is only one independent variable (e.g., the pressure P). The concentrations of the three phases in equilibrium lie on straight lines which form a ruled surface in P-T-X space (with the rulings parallel to X). The projection of the ruled surface on to the P-T plane is a univariant, or triple line. We label these using the notation of Tedrow and Lee.[2] For instance b_1hL_2 is the univariant where bcc$_1$, hcp and ^{3}He-rich liquid L_2 coexist.

Below T_{tr}, isotopic phase-separation occurs between hcp and bcc$_2$; above T_{tr}, separation into hcp and bcc$_1$ or into bcc$_1$ and bcc$_2$ may take place. The equation for the (bcc$_1$ + bcc$_2$) line is, of course, Eq. (7), but the (hcp + bcc$_1$) and (hcp + bcc$_2$) lines were obtained numerically (see Appendix). Alternatively a simple approximation for the (hcp + bcc$_2$) line may be used when the ^{3}He concentration X^h and the ^{4}He concentration $Y^b = 1 - X^b$ are very small;

$$\begin{aligned} k_B T &= \frac{\Delta_3 + A^h(1 - 2X^h)}{\ln[(X^h)^{-1} - 1]}, \quad X^h \ll 1 , \\ &= \frac{\Delta_4 + A^b(1 - 2Y^b)}{\ln[(Y^b)^{-1} - 1]}, \quad Y^b \ll 1 . \end{aligned} \qquad (11)$$

These approximate equations put $X^h \approx Y^b$ and $A^h \approx A^b$ in the small terms, so as to keep their form similar to (7).

Figure 1 shows the experimental values of T_{PS} determined by PSGA at pressures close to 34 atm. Although the data agree fairly well with the theoretical phase diagram, they really should be compared to the theory explained in Sec. II C. This is because the measurements were made quickly without allowing equilibrium with respect to crystal structure to be attained.

We have also calculated the volume and pressure changes accompanying the phase separation for the concentrations X_0 in the PSGA experiment and the specific heats which would have been observed in the EMD experiment. Some of the volume changes are compared with the PSGA measurements in Table I. The agreement is quite satisfactory, and this includes the data at

TABLE I. Comparison between regular solution theory and solid phase-separation data.

X (%)	P (atm)	T_{PS}^{app} (Measured) (K)	T_{PS}^{app} (Theory) (K)	$v(0)-v(T_{PS})$ (Measured) (mm³/mol)	$v(0)-v(T_{PS})$ (Theory) (mm³/mol)	Reference, remarks
			Metastable fitted points			
8.4	33.5	0.31±0.01	0.310	−46±4	−49	PSGA (Ref. 7) $f^h=0.82$
16.6	35.4	0.345±0.01	0.345	−29±3	−29	PSGA (Ref. 7) $f^h=0.56$
		Other fitted points, treated as equilibrium measurements				
0.84	32.35	0.189±0.005	0.185	−4.4	−4.5	Iwasa and Suzuki (Ref. 27) hcp precipitating bcc
99.13	32.8	0.158±0.005	0.1605	−3.3	−3.1	Iwasa and Suzuki (Ref. 17) bcc precipitating bcc
		Comparison with some other data (not used in the fit)				
3.0	28.6	0.27	0.251	−14	−16	PSGA (Ref. 7) hcp precipitating bcc (treated as equilibrium)
48.5 →	31.5	0.38	0.389	−109	−91	PSGA (Ref. 7) metastable, $f^h\sim0$
	38.5	0.37	0.374	−76	−91	PSGA (Ref. 7) metastable, $f^h\sim0$
92.8	33.9	0.255	0.266	−31	−24	PSGA (Ref. 7) metastable, $f^h\sim0$
99.61	33.8	0.138	0.142	−1.7	−1.4	PSGA (Ref. 7) metastable, $f^h\sim0$

$X_0 = 8.4\%$ and 16.6% which agree with the theory explained in Sec. II C. On the other hand the specific heat calculated assuming that the hcp-bcc transformation is in equilibrium disagrees greatly with the EMD data. This implies that their samples (which were contained in a copper sinter with 10-μm pores) remained bcc throughout the experiment.

C. Phase separation in metastable hcp-bcc mixtures

According to the equilibrium phase diagram in Fig. 1, a solid mixture cooled to low temperatures separates into two phases of different crystal structure. In the experiments of PSGA the crystalline transformation was observed to take place very slowly compared to the separation of the isotopes. After an unspecified period at low temperatures the data were taken while warming at a rate which was fast compared to the rate of crystalline transformation. In other words the fraction f^h of the sample which was in the hcp phase did not change appreciably during the measurements. In these circumstances only partial thermodynamic equilibrium is achieved. The appropriate equation is

$$\mu_3^h - \mu_4^h = \mu_3^b - \mu_4^b \quad (f^h \text{ fixed}) . \tag{12}$$

This assumes that the bcc phase (or phases) can exchange a ^{3}He for a ^{4}He in the hcp phase but the total number of atoms in the hcp phase remains constant.

For a bcc mixture of initial concentration X_0, the maximum value of f^h after a long time at $T=0$ is $1-X_0$ (which is the minimum f^h for an initially hcp mixture).

Figure 2 shows the result of applying Eq. (12) and (10) for two of the concentrations used by PSGA, with $0 < f^h < 1-X_0$ adjusted in both cases to agree with the observed transition temperature. This figure, which bears a superficial resemblance to Fig. 1, is conceptually quite different from the equilibrium phase diagram. A sample which was originally bcc of concentration X_0 becomes, at $T=0$, separated into three phases; fractions f^h of hcp, $(1-X_0-f^h)$ of bcc₁ and X_0 of bcc₂. As the sample is warmed, the three phases follow the curves marked with the arrows until, at the apparent phase-separation temperature T_{PS}^{app}, the bcc₂ phase disappears. This is marked by a sharp decrease in the rate of change in volume with temperature. Table I shows that the volume changes observed by PSGA agree fairly well with values calculated from our model.

III. DETERMINATION OF THE PARAMETERS IN THE MODEL: THE FREE-ENERGY DIFFERENCE BETWEEN hcp AND bcc

Since we are neglecting the effect of the phonon and spin specific heats, the free-energy differences Δ_3 and Δ_4 between the metastable and stable crystal structures in the pure isotopes and their pressure derivatives, the volume differences $\delta v_3 = \partial \Delta_3/\partial P = v_3^h - v_3^b$ and $\delta v_4 = \partial \Delta_4/\partial P = v_4^b - v_4^h$, are only functions of pressure. In the narrow range of pressure in which isotopic phase separation proceeds rapidly, it would probably be sufficient to treat δv_3 and δv_4 as constants. In pure ^{3}He, extrapolating the data of Straty and Adams[18] to the $T=0$ end of
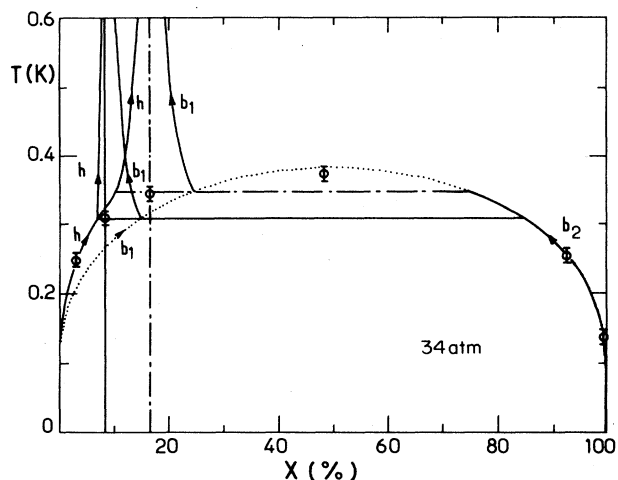
FIG. 2. The coexistence of hcp (h) and bcc (b_1 and b_2) phases in partial equilibrium, according to Eq. (12). The experimental points are from Ref. 7. The fraction of the atoms in the hcp phase f^h is fixed, but the hcp and bcc phases may exchange ^{3}He for ^{4}He or vice versa. The curves shown are for two of the samples in Ref. 7 of average concentrations $X_0 = 8.4\%$ and $X_0 = 16.6\%$ and with $f^h = 0.82$ and $f^h = 0.56$. The average concentrations are shown by the vertical lines. The dotted line is the equilibrium b_1-b_2 phase separation line. At low temperatures the solid consists of three phases h, b_1, and b_2. As the temperature is raised the concentrations in the three phases follow the curves marked by the arrows. At the apparent "phase-separation temperature" T_{PS}^{app}, shown by the horizontal lines, the b_2 phase disappears, leaving two phases h and b_1.

the bcc-hcp transformation line gives $\delta v_3 = \delta v_3^0 \approx -0.09$ cm^3/mol at $P = P_3^0 = 105$ atm. This pressure is much higher than the pressures we are interested in, but we can make use of these data if we assume v_3 to depend linearly on P:

$$\delta v_3 = \delta v_3^0 + \beta_3 (P - P_3^0) \ , \tag{13}$$

so that

$$\Delta_3 = \int_{P_3^0}^P \delta v_3 \, dP' = (P - P_3^0)[\delta v_3^0 + \tfrac{1}{2}\beta_3 (P - P_3^0)] \ , \tag{14}$$

which leaves one parameter β_3 to determine.

For ^{4}He, P_4^0 is clearly less than the melting pressure at $T = 0$, 24.993 atm,[19] otherwise P_4^0 and δv_4^0 are unknown. On the other hand there are many accurate measurements along the hcp-bcc transformation line from the lower triple point with the liquid at 1.463 K and 25.9 atm to the upper triple point at 1.772 K and 29.7 atm. We have reduced these transformation line data to $T = 0$ by allowing for the effect of the thermal phonons. The method is as follows.

Edwards and Pandorf[20] pointed out that S/C_v, the ratio of the entropy to the specific heat in bcc ^{4}He, plotted against T/Θ where Θ is the T-dependent Debye temperature, falls on the same curve as that for ^{3}He at the same molar volume. This implies that the phonon spectra in the two solids have the same general shape. One can

therefore use thermodynamic data[20,21] on bcc ^{3}He to extrapolate the Gibbs free energy of bcc ^{4}He to $T = 0$.

At a point on the transformation line T_t, P_t,

$$g^h(P_t, T_t) = g^b(P_t, T_t) \ , \tag{15}$$

where

$$g(P_t, 0) = g(P_t, T_t) + \int_0^{T_t} S(P_t, T) \, dT \ , \tag{16}$$

and

$$S(P_t, T) \approx S(v_t, T) + (\partial S / \partial P)_T [P_t - P(v_t, T)] \ . \tag{17}$$

We can define the Grüneisen constant γ by writing $(\partial S / \partial P)_T = -(\partial v / \partial T)_P = -v\alpha_T = -\gamma K C_v$ where K is the compressibility, α_T the thermal expansion coefficient, and C_v the specific heat. We assume that γ is independent of T (the Grüneisen law). As shown by Edwards and Pandorf[22] and Gardner et al.[23] this is a very accurate approximation for hcp ^{4}He, and it is a reasonable approximation for bcc ^{3}He.[20,21] Integrating $(\partial P / \partial T)_v = \gamma C_v / v$ with respect to T at constant v gives

$$P_t - P(v_t, T) = (\gamma / v_t)[u_t - u(v_t, T)] \ , \tag{18}$$

where $u_t = u(v_t, T_t)$ is the internal energy per atom.

Combining Eq. (18) with (16) and (17),

$$g(P_t, 0) - g_t = \int_0^{T_t} S(v_t, T) \, dT - \tfrac{1}{2}(\gamma^2 K_t / v_t)$$
$$\times [u_t - u(v_t, 0)]^2 \ . \tag{19}$$

In the last term, which is small, we have neglected the T dependence of K.

For hcp ^{4}He the right-hand side of (19) is easily evaluated from tables of the "reduced" thermodynamic functions, $S(\tau)$ and $(u - u_0)/k_B T$ as a function of $\tau = T/\Theta_0(v)$ or $T/\Theta_{05}(v)$, given in Refs. 22 and 23. The important assumption that we make, based on Edwards and Pandorf's remark about S/C_v, is that this procedure can also be applied to bcc ^{4}He using tables from the data[20,21] for bcc ^{3}He at the same molar volume. Starting from S or C_v at the transformation line, one finds from the tables $\tau = T_t / \Theta_0$ giving Θ_0. The value of γ is found from α_T, C_v, K etc. at the transformation line.

In a similar way, we can correct the volumes of bcc and hcp ^{4}He on the transformation line to $T = 0$ using

$$v(P_t, 0) = v(P_t, T_t) - \gamma K_t [u_t - u(v_t, 0)] \ . \tag{20}$$

To estimate the uncertainty in our procedure we also used the hcp ^{4}He tables (rather than bcc ^{3}He) to correct the bcc ^{4}He data, giving the error bars on the results in Fig. 3.

Figure 3(a) shows that, in the pressure range of interest, it is sufficiently accurate to take $\delta v_4 = v_4^b - v_4^h = \delta v_4^0 = 0.16$ cm^3/mol, a constant. With δv_4^0 as the slope of the straight line in Fig. 3(b), the difference in Gibbs functions is

$$\Delta_4 = g_4^b - g_4^h = \delta v_4^0 (P - P_4^0) \ , \tag{21}$$

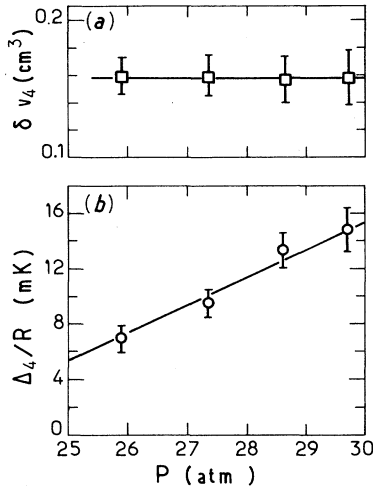where $P_4^0 = (22.2 \pm 1)$ atm. This would be the hcp-bcc transformation pressure in pure ^{4}He at $T = 0$ if the liquid

FIG. 3. (a) The molar volume difference $\delta v_4 = v_4^b - v_4^h$ between bcc and hcp pure ^{4}He at $T = 0$, as a function of pressure. The squares and their errors were calculated from experimental data as described in the text. The horizontal line is $\delta v_4 = 0.16$ cm^3/mol. (b) The difference in Gibbs function $\Delta_4 = g_4^b - g_4^h$ between bcc and hcp pure ^{4}He at $T = 0$. The straight line represents Eq. (21) with $\delta v_4 = 0.16$ cm^3/mol and $P_4^0 = 22.2$ atm. The calculation of the circles from experimental data is described in the text.

did not have a lower free energy than the solid. In analyzing the data on phase separation in solid mixtures in Table I, we have used (21) up to ~ 36 atm.

The other parameters in the theory, β_3 in (13) and (14) and A^h, B^h and A^b, B^b were fitted to the first four points in Table I, and to a limited extent, to data on the hcp-bcc transformation in mixtures. The mixture data are the following.

Grigoriev et al.[24] observed coexistence between hcp and bcc at $P = 34$ atm and $T = 0.5$ K in a sample with $X_0 = 6.3\%$. In contrast with Grigoriev et al., Miyoshi et al.[25] observed coexistence at 1 K over a range of pressure, as one would expect. For $X_0 = 7.78\%$ they found coexistence from ~ 30 to ~ 37 atm (our calculated range is 27.4 to 28.3 atm) and for $X_0 = 32.1\%$ they observed ~ 45 to ~ 51 atm (we calculate 43.5 to 46.5 atm). At higher pressure and concentration Vignos and Fairbank[26] observed coexistence for $X_0 = 75\%$ at $p = \sim 80$ to ~ 83 atm. Our calculated range for this concentration is 76 to 79 atm.

There are serious discrepancies between the coexistence data at low pressure and the theory, particularly with the measurements of Grigoriev et al. We cannot explain the discrepancies, except to remark that PSGA showed that equilibrium with respect to crystal structure is attained very slowly.

Two important fitted points in Table I are those of Iwasa and Suzuki.[17,27] In these experiments the approach to equilibrium was carefully monitored by both ultrasonic and pressure measurements. It was observed that, in general, there are three processes taking place after a change in temperature; isotopic phase separation

(or remixing if the temperature is increased), the hcp-bcc transformation, and the relief of the strain caused by the first two processes by the production of dislocations. All three of these processes were studied in rapid and slow warming and cooling.

In fitting the parameters of the model we found little advantage in using different values for A^h and A^b, even when using a larger number of data than in Table I, with a more complicated volume dependence for Δ_4. Therefore we have taken $A^h/k_B = A^b/k_B = 0.76$ K at 35.8 atm, the value found by EMD. The fitted value of $B^h = B^b$ is -0.364 cm^3/mol, in good agreement with that found by Ehrlich and Simmons,[16] $B = -(0.43 \pm 0.13)$ cm^3/mol. In arriving at this estimate they considered a wide range of other experiments.[7,13,28-31] These results are somewhat lower than the recent determination by Fraass and Simmons,[14] $B = -0.54$ cm^3/mol.

The fitted value of β_3 is such that δv_3 changes from $\delta v_3^0 = -0.09$ cm^3/mol at $P_3^0 = 105$ atm to -0.176 cm^3/mol at 35.8 atm.

IV. CALCULATION OF THE PHASE DIAGRAM: THE LIQUID PHASES

A. The ^{3}He-rich liquid L_2

To complete the phase diagram we need expressions for the chemical potentials in the liquid phases. The ^{3}He-rich liquid L_2 is straightforward since $(1 - X)$, the concentration of ^{4}He, is small in the whole temperature range $(X > 0.95)$. According to the Zharkov-Silin theory[32] the dissolved ^{4}He behaves like a gas of quasiparticles of mass m_4^* so that

$$\mu_4(P, T, X) = g_4^L(P) + E_4 + k_B T \ln[(T_4^*/T)^{3/2}(1 - X)] .$$

(22)

Here $E_4(P)$ is the difference in chemical potential for one ^{4}He atom in liquid ^{3}He at $T = 0$ compared to liquid ^{4}He at $T = 0$. The temperature $T_4^*(P)$ is defined by

$$k_B T_4^* = (2\pi\hbar^2/m_4^*)/(v_3^L)^{2/3} ,$$

(23)

where v_3^L is the volume per atom in pure liquid ^{3}He. Although the ^{4}He quasiparticles are bosons, Boltzmann statistics are used in (22), since the concentration of ^{4}He vanishes exponentially as $T \rightarrow 0$.

The first term in (22), $g_4^L(P)$, is the chemical potential of pure liquid ^{4}He. In terms of g_4^h, the chemical potential in pure hcp ^{4}He, which we use as the "standard" or reference state for ^{4}He

$$g_4^L(P) = g_4^h(P) + \int_{P_4^m}^{P} (v_4^L - v_4^h) dP' .$$

(24)

The integrand is the volume difference between liquid and hcp ^{4}He at pressure P', and $P_4^m = 24.993$ atm is the melting pressure. All the properties of pure ^{4}He, g_4^L, g_4^h, v_4^L, v_4^h, P_4^m are independent of the temperature, since we are presently neglecting thermal phonons. Phonon effects are considered in Sec. IV E.

The quantities $E_4(P)$ and $T_4^*(P)$ have been determined by Laheurte[33] between $P = 0$ and $P = 20$ atm. Laheurte

found that $T_4^* = 1.114$ K could be taken as independent of P. Extrapolating his results for $E_4(P)$ to 25 atm, gives $E_4 = (0.476 \pm 0.005)$ K with negligible pressure dependence in the range of interest to us.

To represent the integral in (24) conveniently, we take

$$v_4^L - v_4^h = (2.165 \text{ cm}^3/\text{mol})[1 - (P - P_4^m)/(83.3 \text{ atm})] \tag{25}$$

from a fit to the data of Grilly.[19]

The ^{3}He chemical potential in L_2 is obtained from the Gibbs-Duhem relation and Eq. (22);

$$\mu_3(P,T,X) = g_3^L(P,T) + k_B T \ln X , \tag{26}$$

where g_3^L is related to g_3^b, the reference state for ^{3}He, by

$$g_3^L(P,T) = g_3^b(P,T) + \int_{P_3^m(T)}^{P} [v_3^L(P',T) - v_3^b(P',T)] dP' . \tag{27}$$

We used Greywall and Busch's polynomial representation[34] for the ^{3}He melting curve $P_3^m(T)$ up to the minimum ($T_{\min} = 0.318$ K) and a simple quadratic fit to Grilly's data[35] from the minimum up to 0.8 K. The temperature dependence of $v_3^L(P',T)$ was included in the integral using data from Refs. 35–37,

$$v_3^L(P,T) - v_3^b(P,T) = (1.241 \text{ cm}^3/\text{mol})$$
$$\times [1 - (P - P_{\min})/(157.4 \text{ atm})$$
$$- (T - T_{\min})/(5.26 \text{ K})] . \tag{28}$$

For $0 \leq T \leq 0.07$ K, the term linear in T in (28) was smoothly joined to one proportional to T^2.

B. The ^{4}He-rich liquid L_1

Although the ^{4}He-rich liquid L_1 has been studied more extensively than any other phase of ^{3}He-^{4}He mixtures, the task of accurately representing the chemical potentials in L_1 is more difficult than in the other phases. This is because the concentration becomes as high as 22% at 0.5 K on the $b_1 L_1 L_2$ univariant and most theoretical and experimental work on L_1 has been concerned with low temperatures and concentrations.

The formulas for μ_3 and μ_4 we use are[38]

$$\mu_3(P,T,X) = g_3^L(P,0) + E_3(P) + \Delta g_F(T,T_F^*)$$
$$+ k_B T_{F0}^* [1 - \chi p_F^2/(m_4 s)^2]$$
$$+ \tfrac{1}{2} x (V_0/v_4^L) + (1+\alpha)(\mu_4 - g_4^L) , \tag{29}$$

and

$$\mu_4(P,T,X) = g_4^L(P) + \tfrac{2}{3}\Delta u_F(T,T_F^*)$$
$$+ \tfrac{3}{5} k_B T_{F0}^* [1 - \tfrac{10}{7}\chi p_F^2/(m_4 s)^2]$$
$$+ \tfrac{1}{4} x^2 (V_0/v_4^L) . \tag{30}$$

The pressure range for which we need (29) and (30) is rather narrow, from about 24 atm to about 26 atm. Consequently, in the following, most of the quantities have

been taken as pressure independent. Unfortunately the highest pressure at which the single-phase properties of L_1 have been studied is 20 atm. The highest concentration at which single-phase data are available is $\sim 12\%$.

The various quantities appearing in (29) and (30) are as follows: $E_3(P)$ is the difference in free energy for one ^{3}He atom in liquid ^{4}He compared to liquid ^{3}He at $T = 0$. The quantity $x = X/(1 + \alpha X) = n_3 v_4^L$ is the ratio of the number density of ^{3}He in the mixture to that of ^{4}He in pure ^{4}He at the same pressure. The "BBP parameter" α [which also gives the pressure variation of $E_3(P)$ through $\partial E_3/\partial P = (1+\alpha)v_4(P) - v_3(P)$] is taken to be 0.165 by extrapolation from Watson et al.[39] The velocity of sound[40] $s = 366$ m/s is taken to be independent of pressure. The Fermi temperature T_{F0}^* defined by

$$k_B T_{F0}^* = p_F^2/2m_{03}^* = \hbar^2(3\pi^2 n_3)^{2/3}/2m_{03}^* \tag{31}$$

calculated with $m_{03}^* = 3.0m_3$ from Ref. 41, is used to calculate the $T = 0$ contributions to the chemical potentials. The other Fermi temperature T_F^*, calculated with $m_3^* = 3.3m_3$ from the results of Landau et al.,[41] is used to calculate the temperature-dependent contributions. (The use of two effective masses in this way is part of the "Fermi-entropy" model, see Refs. 38, and 41).

The functions $\Delta g_F(T,T_F^*) = g_F(T,T_F^*) - g_F(0,T_F^*)$ and $\Delta u_F = u_F(T,T_F^*) - u_F(0,T_F^*)$ are the temperature-dependent parts of the Gibbs and internal energies of an ideal Fermi gas with Fermi temperature T_F^*. They were obtained from the polynomials given by Owers-Bradley et al.[42] The small terms in χ are due to the nonparabolic form of the quasiparticle energy.[38] The dimensionless parameter χ, which has not been determined under pressure, was taken as 0.2, its approximate value at $P = 0$.[38,43] The terms in χ are rather small and they have little effect on the results.

The term $(1+\alpha)(\mu_4 - g_4^L)$ in (29) ensures that μ_3 and μ_4 satisfy the Gibbs-Duhem relation. If this relation is not exactly satisfied the chemical potentials do not represent tangents to a Gibbs free-energy surface, giving problems in finding phase equilibrium.

In terms of the ^{3}He reference state, bcc ^{3}He at P and T,

$$g_3^L(P,0) = g_3^b(P,T) + k_B T \ln 2$$
$$+ \int_{P_3^m(0)}^{P} [v_3^L(0) - v_3^b(0)] dP' , \tag{32}$$

where $P_3^m(0)$ is 33.95 atm.[34] The first two terms on the right-hand side of (32) represent $g_3^b(P,0)$.

In writing Eqs. (29) and (30) we have taken a very simplified form of the effective interaction between ^{3}He quasiparticles, namely $V(\mathbf{p}_1,\mathbf{p}_2,q) = V_0$, a constant. More precise analyses[38,44] of data at lower pressures have assumed various forms, e.g., a dipolar interaction proportional to $\mathbf{p}_1 \cdot \mathbf{p}_2$, polynomials in q etc. Apart from the large number of parameters to be determined, these forms gave problems at high X, because the L_1 phase usually became intrinsically unstable, i.e., $\partial^2 G/\partial X^2 < 0$, for plausible values of the parameters. The intrinsic stability of L_1 seems to put quite stringent conditions on the interaction, and we were able to achieve a satisfactory fit only with $V(\mathbf{p}_1,\mathbf{p}_2,q) = V_0$, a constant.

Once the simple form of the interaction was decided upon, we used the properties of L_1 at the end of the hL_1L_2 univariant at $T=0$ to determine the values of $(V_0/v_4^L)/m_4s^2$ and $E_3(P)$. According to the recent freezing curve measurements of Lopatik,[45] the end of the univariant occurs at a concentration X_{sat} in L_1 which is not less than 8% and at a pressure $p^*=25.29$ atm. This maximum concentration X_{sat} is consistent with extrapolation of the results of Landau *et al.* and Watson *et al.* The pressure p^* is related[46] to π_{sat}, the osmotic pressure[41] of L_1; since L_1 is in equilibrium with the hcp phase (which at $T=0$ is pure ^{4}He)

$$\mu_4^{L_1}(p^*,X_{sat},0)=g_4^L(p^*)-\pi_{sat}^*v_4^L=g_4^h(p^*) .$$

Using (24) to relate g_4^L to g_4^h, and ignoring the small changes in volume between p^* and p_4^m,

$$p^*=p_4^m+\pi_{sat}^*v_4^L/(v_4^L-v_4^h) . \tag{33}$$

The p^* found by Lopatik corresponds to $\pi_{sat}^*v_4^L/k_B=7.8$ mK, assuming that the freezing pressure of pure ^{4}He is $p_4^m=24.993$ atm. On the other hand, extrapolation of the data of Landau *et al.* gives 9.3 mK, a discrepancy which is probably outside the experimental error. [Lopatik states that his pressure measurements are consistent with the osmotic pressure measurements of Landau *et al.*, but this seems to be based on a comparison made with the volume of L_1 substituted for v_4^L in the denominator of (33), which is not correct.] Since the effect of the discrepancy on the phase diagram is small and Lopatik's results do not involve extrapolation from lower pressures, we have used his π_{sat}^* and X_{sat} to obtain $(V_0/v_4^L)/m_4s^2=-0.053$ [corresponding to $(V_0/v_4^L)/k_B=-3.38$ K] and $E_3/k_B=-0.273$ K at $p^*=25.289$ atm, the values used in our calculations. According to Baym's theory (see Ref. 38 for instance) the BBP parameter α and V_0 are related: $(V_0/v_4^L)/m_4s^2=-\alpha^2=-0.0272$, but since we are using V_0 as a sort of average for $V(\mathbf{p}_1,\mathbf{p}_2,q)$ this may not be a serious discrepancy. In any case, the phase diagram is not very sensitive to V_0.

C. The phase diagram: Univariants, quadrupole points, and freezing curves

The results for the projection of the univariants and quadrupole points on to the P-T plane are shown in Fig. 4, together with some experimental data.[2,3,6,45,47,48] Figure 5 shows some of the univariants in P-T-X space. In discussing the quadrupole points it is convenient to use the notation $(-L_1)$ for $Q1$, $(-b_2)$ for $Q2$ and $(-h)$ for $Q3$ rather than the traditional $Q1, Q2, \ldots$ originating in the pioneering work of Tedrow and Lee. (In any case Vvedenskii[3] and Lopatik[45] seem to have interchanged $Q1$ and $Q2$). Our notation refers to the one phase (out of the five L_1, L_2, b_1, b_2, and h) which is missing from the equilibrium at a given quadrupole point. The separation of hcp into h_1 and h_2 does not occur until the pressure is above that of the critical point $(h_1=h_2,b_2)$, which is at 83 atm, so only h needs to be considered in connection with the quadrupole points.

The possibility of a third quadrupole point $Q3$ or $(-h)$ is implicit in the work of Vvedenskii. On the basis of his experiments he asserted that the three univariants $b_1b_2L_2$, $b_2L_1L_2$, and bL_1L_2 meet at about 0.38 K and 25.7 atm, near the critical line $(b_1=b_2)$. This is the vicinity of the point marked C_1 in Fig. 4. [The notation bL_1L_2 instead of $b_1L_1L_2$ or $b_2L_1L_2$ is used because, above the critical line $(b_1=b_2)$, which in the regular solution theory is given by $k_BT(P)=A^b(P)/2$, there is no distinction between b_1 and b_2.]
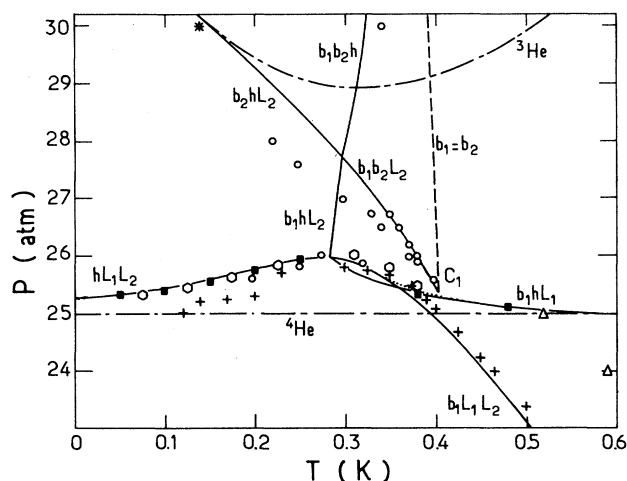
According to the thermodynamics of a binary mix-

FIG. 4. Projection of the phase diagram of liquid and solid ^{3}He-^{4}He mixtures in the P-T plane. The five different phases are: ^{4}He rich liquid (L_1), ^{3}He rich liquid (L_2), ^{4}He rich bcc solid (b_1), ^{3}He rich bcc solid (b_2), and hcp solid (h). According to the phase rule three of these phases may coexist on univariants (the solid curves) and four may coexist at the two quadrupole points where four univariants meet. The univariant b_2hL_2 ends at $T=0$ where it meets the pure ^{3}He melting curve (dot-dash) tangentially. At the point $C1$, the univariant $b_1b_2L_2$ terminates the critical line $b_1=b_2$ (broken line) for phase separation of the bcc solid into b_1 and b_2. [A third quadrupole point $(-h)$ would exist if the $b_1b_2L_2$ line met the $b_1L_1L_2$ line instead of ending on the critical line.] An azeotropic line is shown dotted. It starts and ends tangentially on $b_1L_1L_2$ (at 0.34 K, $X^{b_1}=X^{L_1}\approx15\%$) and on b_1hL_1 (at 0.41 K, $X^{b_1}=X^{L_1}\approx5\%$). The crossing of these two univariants around 0.36 K occurs only in the P-T plane and does not represent a meeting in P-T-X space (see Fig. 5). The experimental points are from Brandt *et al.* (Ref. 47, hexagons), Edwards *et al.* (Ref. 6, star), Lopatik (Ref. 45, rectangles), Tedrow and Lee (Ref. 2, circles), Vvedenskii (Ref. 3, crosses), and Zinovieva (Ref. 48, triangles). There is excellent agreement between the calculated hL_1L_2 and b_1L_1h univariants and the recent work of Lopatik. Vvedenskii's results for the $b_1L_1L_2$ univariant and the Brandt *et al.* results for the hL_1L_2 univariant also agree well with the theory. In drawing their phase diagram Tedrow and Lee apparently labeled their measurements of $b_1b_2L_2$ as belonging to b_1hL_2. The point at 0.14 K, 30 atm was obtained by Edwards *et al.* for $b_1L_2b_2$ in metastable equilibrium. However, the theoretical metastable $b_1L_2b_2$ univariant is hardly distinguishable from the stable hL_2b_2 univariant drawn here.
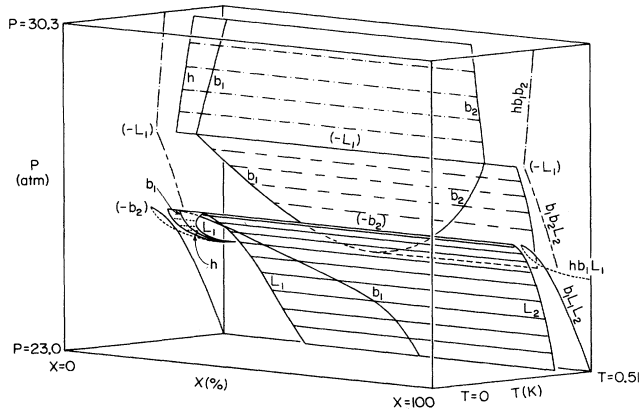
FIG. 5. Four of the univariants, drawn as projections in Fig. 4, shown in P-T-X space. The projections of the univariant surfaces on to the P-T planes are also shown.

ture[49,2] a single univariant can end a critical line (as does $b_1b_2L_2$ in our diagram), while four univariants can meet at a quadrupole point. So Vvedenskii's observations can be interpreted in two ways as follows.

(a) The four univariants $b_1b_2L_2$, $b_1L_1L_2$, $b_2L_1L_2$, and $b_1b_2L_1$ meet at a quadrupole point $Q3$ or $(-h)$ near $C1$. The univariant $b_1b_2L_1$ is very short and terminates the critical line $(b_1=b_2)$.

(b) The situation is as predicted by our calculation and shown in Fig. 4. The univariant $b_1b_2L_2$ terminates the critical line $(b_1=b_2)$ at the point $C1$, while $b_1L_1L_2$ passes close to $C1$ but does not intersect the critical line. Possibility (a) can be obtained in our model, for instance by increasing E_4 (the energy of a ^{4}He atom in ^{3}He) to a large value $E_4 \sim 0.7$ K, but this is quite incompatible with the results of Laheurte.[33]

For all plausible sets of parameters we have used, (b) prevails and $Q3$ does not exist.

With regard to the two other quadrupole points, given in Table II, the agreement for $Q2=(-b_2)$ between our calculation and the measurements of Lopatik $(P=26.0$

atm and $T=0.28$ K) is excellent. Brandt et $al.$[47] found $(-b_2)$ at $(P=26.0$, $T\approx0.30)$, while Tedrow and Lee assumed it to be at $(P=26.0$, $T=0.37$ K) from an extrapolation of the hL_1L_2 univariant. The position of the upper quadrupole point $Q1=(-L_1)$ was proposed as $(P=26.75$ atm and $T=0.33$ K) by Tedrow and Lee, which does not agree well with our calculation (27.72 atm, 0.296 K). The temperatures of $(-b_2)$ and $(-L_1)$ depend mainly on the ratio of the free-energy differences Δ_4/Δ_3. A reduction of Δ_3, corresponding to a less negative β_3, would raise both temperatures by roughly equal amounts. This would also reduce the pressure at $(-L_1)$ as the univariant b_2hL_2 would be extended to higher temperatures. (Note that univariants can be extended beyond the quadrupole point where they terminate in equilibrium. The extensions represent metastable states where the fourth phase which appears at the quadrupole point has not been nucleated).

Although a change in Δ_4/Δ_3 might reduce the disagreement with Tedrow and Lee's estimation of $(-L_1)$, it would also spoil the agreement with Lopatik's measurements of the temperature of $(-b_2)$. Because of these uncertainties, further experiments would be desirable. They need not be direct measurements of $(-L_1)$, for instance measurements on the univariant b_1hL_2 could give the information required. Easier still would be freezing curve measurements (hL_2) and (b_2L_2) in the vicinity of the b_1hL_2 univariant.

The fit between our calculation and Lopatik's measurements of the freezing curves for dilute mixtures is shown in Fig. 6. The agreement is within ±0.1 atm.

Figure 4 shows that the univariant b_1hL_1 approaches $(-b_2)$ from below $b_1L_1L_2$. This feature of the phase diagram was discovered by Lopatik.

In other respects our calculated phase diagram is not very different from the traditional version originally drawn by Tedrow and Lee. It does not agree with the recent proposals of Fraass and Simmons[14] who have tentatively suggested changes in the relative positions of the univariants at low pressures. Our calculated pressures, temperatures and concentrations on the univariants are given in Table III.

TABLE II. Calculated temperatures, pressures (in atm) and concentrations (in %) at critical and quadrupole points, at the ends of azeotropic lines, and at the minimum pressure for the hcp structure.

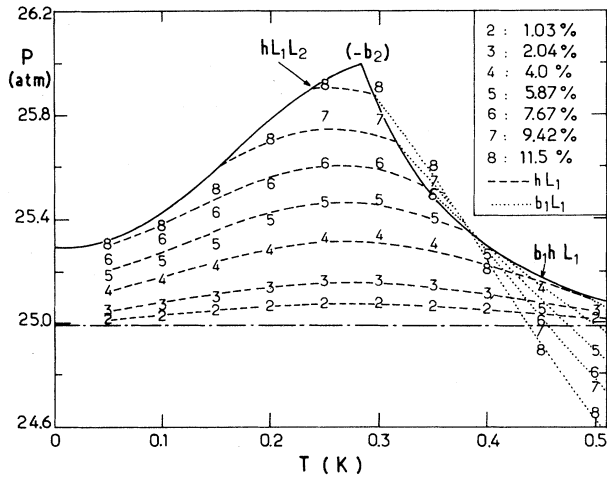| Point	T	P	X^{L_1}	$(1-X^{L_2})$	X^h	X^{b_1}	$(1-X^{b_2})$
$Q1$ or $(-L_1)$	0.296	27.72		2.1	5.4	10.9	10.9
$Q2$ or $(-b_2)$	0.283	26.00	12.9	2.1	3.7	7.3	
$C1$ or $(b_1=b_2,L_2)$	0.403	25.35		5.5		50	50
$C2$ or $(b_1=b_2,h)$	0.376	37.7			14.2	50	50
$C3$ or $(h_1=h_2,b_2)$	0.275	83.0			50		11.0
$(X^{b_1}=X^{L_1},L_2)$	0.337	25.68	14.7	3.5		14.7	
$(X^{b_1}=X^{L_1},h)$	0.411	25.26	5.1		3.4	5.1	
$(X^h=X^{L_1},b_1)$	0.572	25.01	3.38		3.38	4.40	
$(X^h=X^{L_1}\to0)$	0.61	24.989	0		0		
Minimum in b_1hL_1	0.85	24.868	2.33		2.71	3.24	

FIG. 6. Freezing curves for various ^{3}He concentrations. The dashed (hL_1) and dotted (b_1L_1) curves represent our calculation while the numbers represent the data of Lopatik (Ref. 45) at various ^{3}He concentrations. The solid lines are the univariants hL_1L_2 and b_1hL_1 which meet at the quadrupole point $(-b_2)$. The dashed-dot curve is the freezing (melting) curve of pure ^{4}He.

D. Azeotropic lines

An interesting feature noticed by Lopatik[45] is the line of equal concentration or "azeotropic line," $X^{b_1}=X^{L_1}$, shown dotted in Fig. 4. One point on this line can be seen in the T-X diagram at $p=25.6$ atm in Fig. 7. (The data in this figure are from Refs. 1, 2, 45, and 50.) The point A at the maximum of the L_1 region is a point on the azeotropic line. Among other possibilities an azeotropic line may begin or end on a univariant which it must meet tangentially.[49] According to our calculations, the line shown in Fig. 4 joins $b_1L_1L_2$ at ~ 0.34 K where $X^{b_1}=X^{L_1}\approx 15\%$ and b_1hL_1 at ~ 0.41 K where $X^{b_1}=X^{L_1}\approx 5\%$ (see Table II).

Another azeotropic line, $(X^h=X^{L_1})$, which was discovered by Le Pair et al.,[1] begins on the b_1hL_1 univariant at 0.572 K where $X^h=X^{L_1}=3.4\%$ (see Table II). This line ends on the melting curve of pure ^{4}He which it meets at 0.61 K.

Since this azeotrope occurs at low concentrations in both h and L_1, and at comparatively high temperature, it is possible to obtain its asymptotic form analytically. Equating μ_3 in h and L_1, with concentration $X \ll 1$ in both phases, and using (10), (29), and (32)

$$A^h(1-2X)+k_BT\ln X+\Delta_3$$

$$=k_BT\ln 2+\int_{P_3^m(0)}^{P_4^m(T)}[v_3^L(0)-v_3^b(0)]dP$$

$$+E_3+g_F(T,T_F^*)+X(V_0/2v_4^L) , \quad (34)$$

where we have dropped terms in X^2 etc. All pressure-dependent quantities are evaluated at $P=P_4^m$ in (34) be-

cause $(P-P_4^m)$ is second order in X. Writing the first two terms in the high-temperature expansion for g_F:

$$g_F(T,T_F^*)=k_BT\ln[X(T_3^*/T)^{3/2}]+Xk_BT(T_3^*/2T)^{3/2} , \quad (35)$$

where

$$T_3^*=(2\pi\hbar^2/m_3^*)/[2v_4^L)^{2/3}k_B]=1.696 \text{ K} ,$$

one obtains

$$X[2A^h+V_0/2v_4^L+k_BT(T_3^*/2T)^{3/2}]$$

$$=A^h+\Delta_3-E_3-k_BT\ln[2(T_3^*/T)^{3/2}]$$

$$+\int_{P_3^m(0)}^{P_4^m(T)}[v_3^L(0)-v_3^b(0)]dP' . \quad (36)$$

For $X=0$, the solution of this equation is $T=T_0\approx 0.61$ K. Equation (36) has the form $Xf_1(T)=f_2(T)$ where f_1 and f_2 are functions of temperature and $f_2(T_0)=0$. Expanding both f_1 and f_2 in $(T-T_0)$ gives the asymptotic form of the azeotropic line

$$X=(T-T_0)f_2'(T_0)/f_1(T_0)$$

where

$$f_2'(T_0)/k_B=\tfrac{3}{2}-\ln[2(T_3^*/T_0)^{3/2}]$$

and where we have neglected small terms proportional to dP^m/dT evaluated at T_0. We find $f_1(T_0)/k_B\approx 0.926$ K, so that $X\approx(T-T_0)/(1.27$ K) for small X.

E. Freezing and melting lines for nearly pure ^{4}He or ^{3}He

Since the melting curve of pure ^{4}He has a shallow minimum near $T_{4_{\min}}=0.775$ K, the form of the phase diagram for small concentrations of ^{3}He is quite complicated. We show a series of T-X diagrams at closely spaced pressures in this region in Figs. 7, 8, 9, and 10. (These diagrams take thermal phonons and rotons into account in a way described below.)

An interesting feature of the phase diagram in this region is the minimum in the univariant bhL_1 versus pressure. [See Table II and Fig. 9(a).] The minimum corresponds to the lowest pressure, 24.868 atm according to our calculation, at which hcp solid may exist. There is also a minimum pressure for the existence of bcc solid. The bcc minimum occurs in a region of concentration in the liquid which is too far from 0 or 1 for our models to be accurate, and we have not attempted to calculate it.

The temperature dependence of the ^{4}He melting pressure $P_4^m(T)$ is of course due to the thermally excited rotons in liquid ^{4}He and the phonons in both the solid and the liquid. We have taken these effects into account in the calculation of the phase diagram near melting for small concentrations of ^{3}He. For $P_4^m(T)$ we used a quadratic interpolation between the tabulated values given by Grilly. Then terms representing the phonon contributions to the Gibbs energies were inserted in $g_4^h(T)$ and $g_4^b(T)$. The temperatures at which these terms are significant are high enough that the Debye theory is

TABLE III. Calculated temperatures, pressures, and concentrations (in %) on the univariants.

T (K)	P (atm)	X^{L_1}	$(1-X^{L_2})$	X^h	X^{b_1}	$(1-X^{b_2})$
		(hL_1L_2)				
0	25.29	8.0	0	0		
0.12	25.50	8.8	0.06	0.02		
0.18	25.72	10.0	0.41	0.40		
0.24	25.92	11.6	1.22	1.8		
		$(b_1L_1L_2)$				
0.32	25.81	14.1	3.0		11.9	
0.38	25.21	16.3	4.9		24.2	
0.44	24.22	18.8	7.1		46.5	
0.50	23.14	21.8	9.6		52.8	
		(b_1hL_1)				
0.32	25.66	8.9		3.6	6.2	
0.38	25.36	5.9		3.5	5.4	
0.44	25.20	4.6		3.4	4.9	
0.50	25.10	3.9		3.4	4.6	
0.60	24.98	3.1		3.2	4.2	
0.70	24.91	2.8		3.1	3.8	
0.80	24.87	2.5		2.9	3.5	
0.90	24.87	2.2		2.6	3.0	
		(b_1hL_2)				
0.29	26.75		2.1	4.5	8.8	
		$(b_1b_2L_2)$				
0.32	27.28		2.7		14.6	14.6
0.36	26.44		3.9		23.5	23.5
0.40	25.43		5.3		42.5	42.5
		(b_2hL_2)				
0.08	31.37		0.0007	0.0013		0.0047
0.12	30.50		0.021	0.052		0.13
0.18	29.52		0.24	0.65		1.3
0.24	28.65		0.91	2.4		4.6
		(b_1b_2h)				
0.32	29.80			7.3	15.5	15.5
0.36	34.88			11.9	29.7	29.7

inadequate. A reasonable fit to the empirical data for hcp ^{4}He and bcc ^{3}He near 1 K is found to be

$$\int_0^T S_{\text{phonon}} dT' \approx a_0 T^\zeta / \Theta_{05}^{\zeta-1} ,\qquad (37)$$

where $\zeta = 4.6$, Θ_{05} is the empirical Debye temperature at $T/\Theta = 0.05$, and $a_0 \sim 86 k_B$ for hcp ^{4}He and $a_0 \sim 125 k_B$ for bcc ^{3}He. The parameter Θ_{05} is related to the atomic volume v by the approximate relation

$$\Theta_{05} = \Theta_s (v/v_s)^{-\gamma} ,$$

with $\gamma \approx 2.6$. Here v_s and Θ_s are the values at an arbitrarily chosen standard pressure P_s. We chose $P_s = P_4^m(0) = 24.993$ atm for ^{4}He and $P_s = P_{3_{\min}}^m = 28.933$ atm for ^{3}He. Finally we used the approximate equation of state

$$v = v_s [1 + \beta K_s (P - P_s)]^{-1/\beta} ,\qquad (38)$$

which is obtained by integration of a simple power-law

dependence of the compressibility on the volume:

$$K = K_s (v/v_s)^\beta .$$

Substituting these equations into (37):

$$\int_0^T S dT' = [a_0 T^\zeta / \Theta_s^{\zeta-1}][1 + \beta K_s (P - P_s)]^{-\gamma(\zeta-1)/\beta} .\qquad (39)$$

Table IV summarizes the various parameters we have assumed for both isotopes and both crystal structures. For consistency the phonon terms in g_3^b and g_3^h have been included, although they have no appreciable effect on the results. All the numerical calculations in this paper include the phonon terms in both pure ^{3}He and ^{4}He.

The inclusion of the phonon terms in the Gibbs energies of the pure solid phases does not take into account the effect of thermally excited phonons on the excess function g_E. We have continued to represent g^E by the regular solution theory, Eq. (3) with A independent of temperature. This means that the theory assumes that

TABLE IV. Parameters characterizing the phonon contributions to the Gibbs energies of hcp and bcc ^{4}He and ^{3}He. Values in parentheses have been assumed from the values for the other crystal structure. The parameters $\gamma = 2.6$ and $\zeta = 4.6$ were the same for all four crystals.

Crystal	P_s (atm)	β	K_s (atm^{-1})	$\frac{a_0}{k_B}$	Θ_s (Kelvin)
hcp ^{4}He	24.993	4.95	0.0038	86	24.6
bcc ^{4}He	24.993	(4.95)	0.0077	(125)	20.3
bcc ^{3}He	28.933	5.52	0.0062	125	12.3
hcp ^{3}He	28.933	(5.52)	($\sim$ 0.0062)	(86)	19.0
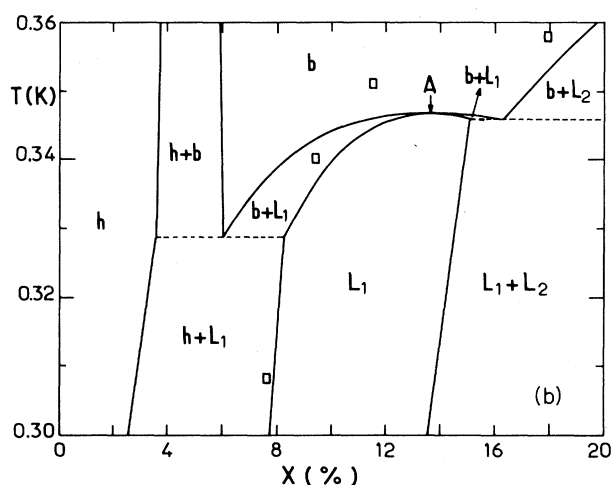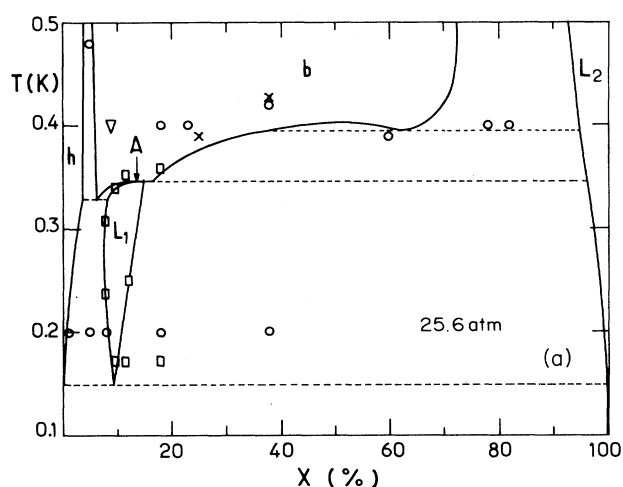
FIG. 7. (a) The T-X phase diagram at 25.6 atm. The experimental points are from Lopatik (Ref. 45, □), Tedrow and Lee (Ref. 2, ○), Le Pair et al. (Ref. 1, ▽), and Weinstock et al. (Ref. 50, ✕). The calculated temperature of the hL_1L_2 three-phase equilibrium at 0.15 K is lower than the measurements of Lopatik (0.17 K) and Tedrow and Lee (0.2 K). An azeotropic point (A) exists where the concentrations in b and L_1 are equal. (b) Enlargement of (a) showing the structure of the phase diagram near the azeotropic point A.

the phonon contribution to g for a mixture is merely a linear interpolation between the pure phases. This is clearly oversimplified but it is probably an adequate approximation for very small concentrations, as required for the calculations of Figs. 9 and 10.

Another interesting part of the phase diagram is the region close to the minimum in the melting curve of pure ^{3}He. Figure 11 shows T versus X at the pressure of the minimum. The shape of our calculated curves is in complete agreement with the theory given by Lifshitz and Sanikidze[51] a long time ago.

We now turn to the problem mentioned in the Introduction, namely the relative solubility of small concentrations of ^{4}He in solid ^{3}He (b_2) and liquid ^{3}He (L_2). Equating μ_4 in the two phases, using (10) and (22) to (24),

$$A^b (X^b)^2 + k_B T \ln(1 - X^b) + \Delta_4$$
$$= E_4 + k_B T \ln[(T_4^* / T)^{3/2}(1 - X^L)]$$
$$+ \int_{P_4^m}^{P} (v_4^L - v_4^h) dP' \ . \tag{40}$$
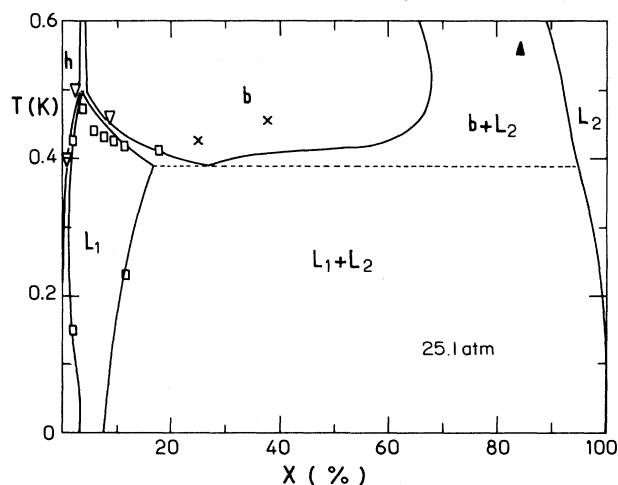
Since X^b and X^L are both close to 1, so that $P \approx P_3^m(T)$,

FIG. 8. The T-X diagram at 25.1 atm. The experimental points are from Lopatik (Ref. 45, □), Weinstock et al. (Ref. 50, ✕), Le Pair et al. (Ref. 1, ▽), and Zinovieva (Ref. 48, ▲).
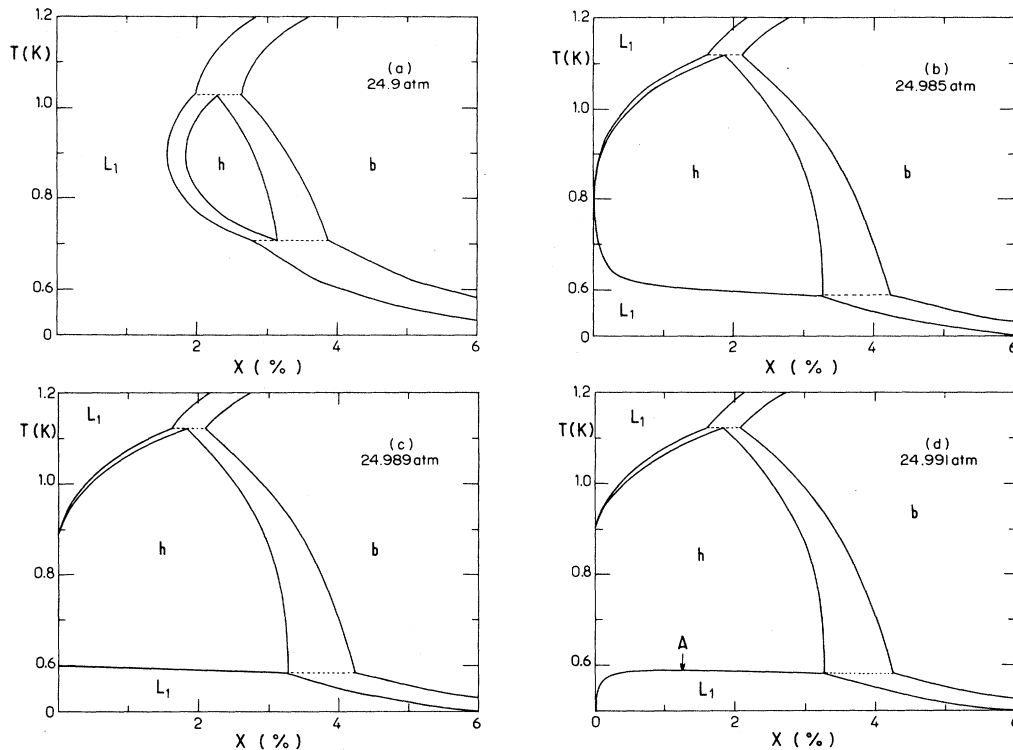
FIG. 9. The existence of an azeotropic line joining the melting curve of pure ^{4}He to the bhL_1 univariant, and minima in both these curves has interesting consequences for the phase diagram near 25 atm (see also Fig. 10). (a) At 24.9 atm, which is above the minimum in bhL_1 at 24.868 atm, an hcp pocket exists inside the region of coexistence of the L_1 and b phases. The two dotted horizontal lines both belong to the bhL_1 univariant. (b) At 24.985 atm, the pressure of the minimum in the melting curve of pure ^{4}He, the freezing and melting curves of the hcp phase are tangent to the pure ^{4}He axis at $T_{min}=0.775$ K. (c) At 24.989 atm, the pressure at which the azeotropic line joins the pure ^{4}He melting curve, an azeotropic point first appears on the T axis [the low-temperature coexistence domain of the h and L_1 phases is so narrow ($\sim$0.25 mK near $X=3\%$) that it is invisible on this scale]. (d) At 24.991 atm, the melting pressure of pure ^{4}He at 0.5 K, the azeotropic point A is at $Xh=XL_1\sim1\%$ and the h phase extends to $T=0.5$ K.
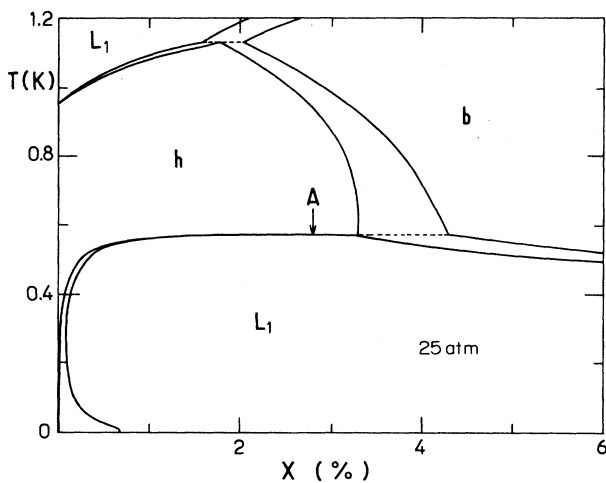

FIG. 10. At 25.00 atm, which is above the freezing pressure of pure ^{4}He at $T=0$ (24.993 atm) but below the pressure (25.01 atm) at which the azeotropic line joins the bhL_1 univariant, the azeotropic point A still exists at $X_h=X_{L_1}=2.8\%$. The hcp phase extends down to $T=0$. The freezing curve starts from a nonzero concentration ($X\sim0.7\%$) at $T=0$. The shape of the phase diagram at lower pressures is shown in Fig. 9 and at higher pressures in Figs. 7 and 8.

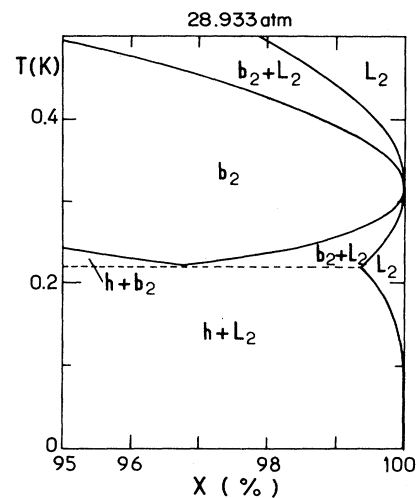FIG. 11. As predicted by Lifshitz and Sanikidze (Ref. 51) the existence of a minimum in the melting curve of pure ^{3}He at $P=28.933$ atm and 0.318 K has a particular effect on the phase diagram of ^{3}He-^{4}He mixtures at the same pressure. Both the melting and freezing lines are tangent to the pure ^{3}He axis. Our calculation shows that ^{4}He is more soluble in solid ^{3}He(b_2) than liquid ^{3}He(L_2). This is connected with the fact that the univariant hb_2L_2 is lower in temperature than the melting curve of pure ^{3}He.

we find

$$(1-X^b)/(1-X^L) \approx (T_4^*/T)^{3/2} \exp[E(T)/k_B T] , \quad (41)$$

where

$$E(T) = E_4 - \Delta_4 - A^b + \int_{P_4^m}^{P_3^m(T)} (v_4^L - v_4^h) dP , \quad (42)$$

and E_4, Δ_4, and A^b are the values at $P_3^m(T)$. At extremely low temperatures where $P_3^m(T) \sim P_3^m(0) = 33.95$ atm, $E(T) \approx E(0) \approx (-0.09 \pm 0.02)$ K where we have taken $E_4 = (0.476 \pm 0.02)$ K at 33.95 atm, extrapolated from the data of Laheurte.

Since E is negative, (41) predicts that, at sufficiently low temperatures, the solubility of ^{4}He in liquid ^{3}He will eventually become larger than in the solid. However this occurs at $T \approx 14$ mK where the maximum solubility in either bcc or liquid ^{3}He is completely negligible. For example the limiting form of the maximum solubility in the solid is found by equating μ_4 in b_2 and in pure hcp ^{4}He at $P_3^m(0)$, giving

$$1 - X^b \approx \exp[-(\Delta_4 + A^b)/k_B T] = \exp(-0.79 \text{ K}/T) .$$

$$(43)$$

At 0.08 K this formula gives $1 - X^b = 5 \times 10^{-5}$ in agreement with the concentration on the univariant $b_2 h L_2$ in Table III. At 14 mK it predicts $(1-X^b) \sim 10^{-25}$. For all practical purposes therefore (41) shows that the solubility of ^{4}He in bcc ^{3}He is always larger than in liquid ^{3}He. This result is relevant to the observed dendritic growth of bcc ^{3}He crystals at low temperature.[4]

V. CONCLUSIONS

One of the principal results of this work is the discovery that the phase diagram of solid mixtures, *including the hcp-bcc transformation,* is well explained by the regular solution model which assumes that "the asymmetry parameter" ϵ in (9) is small. There are certainly some disagreements with experiment but the discrepancies between one experiment and another are frequently just as large. These discrepancies may sometimes be attributed to difficulties in achieving equilibrium, particularly with respect to crystal structure, and to inhomogeneity in concentration and strain. (The effects of dislocations, which are themselves generated by the bcc-hcp transformation and the isotopic phase separation, are very complicated and interesting.[52])

Although the regular solution theory roughly agrees with the theories of Prigogine, Klemens et al., Coldwell-Horsfall and Mullin, the reason why it works so well remains somewhat of a mystery, since the theories apparently predict a large asymmetry. On the other hand the theories do not include the effect of the crystal structure, on which the free energy depends quite strongly.

Another of our results is the determination of the difference in free energy Δ_4 and volume δv_4 between bcc and hcp ^{4}He at $T=0$, for the pressure range from about 25 to 30 atm. The corresponding quantities Δ_3 and δv_3 for pure ^{3}He at $T=0$ have been obtained for pressures in the range from 25 to 35 atm, although with probably more uncertainty. As we have shown, these quantities, with the parameters in the regular solution theory A^h and A^b and their pressure derivatives, specify the properties of solid mixtures completely. They should also prove useful to compare with first-principles calculations of the properties of the pure crystals.

With regard to the part of the phase diagram involving the liquid phases, the agreement with the latest measurements of Lopatik is very good and, with earlier measurements, probably within the experimental uncertainties. The formulas we have used for the chemical potentials in the liquid phases cannot be applied near the tricritical line or the lambda transition and this is one direction in which the calculation could be improved.

A straightforward elaboration of the formulas we have presented would include the effects of ^{3}He spin ordering in the solid phases, and the effect of a magnetic field. The theory could then be applied at much lower temperatures.

APPENDIX

In general, the problem of solving for the pressure, the temperature and the concentrations which correspond to equal ^{3}He and ^{4}He chemical potentials in the various phases in equilibrium was solved numerically using a program called CURFIT.[53] This is a program intended to fit experimental data, $y_i(x_i)$ say, to any arbitrary function $y = f(x, \ldots G_j, \ldots)$ by varying the adjustable parameters G_j. The program fits nonlinear functions of G_j by combining the methods of "steepest descent" with "linearized least squares." It usually converges rapidly and it can be applied to problems other than fitting data. Examples are magnet design (where the "experimental data" are the required fields at specified positions) and the solution of coupled transcendental equations as in the present work.

To find a univariant line, for example, the temperature T can be stepped through a set of values. For each T there are four "data points" with $x_i = i$ and $y_i = 0$. The "function" fitted to these data is $\mu_3^a - \mu_3^b$ for $i = 1$, $\mu_4^a - \mu_4^b$ for $i = 2$, $\mu_3^b - \mu_3^c$ for $i = 3$, and $\mu_4^b - \mu_4^c$ for $i = 4$, where the superscripts a, b, and c refer to the three phases which are in equilibrium. The adjustable parameters $G_1, \ldots, G_4$ in the function correspond to X^a, X^b, X^c, and P. Since concentrations must be between 0 and 1, we define $X^a = \exp[-(G_1)^2]$ etc. to prevent physically meaningless solutions. CURFIT requires subroutines defining the fitted function f and also its partial derivatives $\partial f/\partial G_j$. To avoid algebra we used numerical differentiation for the derivatives:

$$\partial f / \partial G_j = [f\{\ldots(1+\epsilon)G_j\ldots\}$$

$$-f\{\ldots(1-\epsilon)G_j\ldots\}]/(2\epsilon G_j)$$

with ϵ chosen as 10^{-4}. The program ran quite fast in

BASIC on a Hewlett Packard 9845B personal computer. For instance, the univariants and other features shown in Fig. 4 took about ten minutes to calculate and to plot on the screen.

---

*Permanent address: Department of Physics, The Ohio State University, Columbus, OH 43210.

[1]C. Le Pair, K. W. Taconis, R. de Bruyn Ouboter, P. Das, and E. de Jong, Physica 31, 764 (1965).

[2]P. M. Tedrow and D. M. Lee, Phys. Rev. 181, 399 (1969).

[3]V. L. Vvedenskii, Pisma Zh. Eksp. Teor. Fiz. 24, 152 (1976) [JETP Lett. 24, 133 (1976)].

[4]E. Rolley, S. Balibar, and F. Gallet, Europhysics Lett. 2, 247 (1986).

[5]See, e.g., A. H. Wilson, Thermodynamics and Statistical Mechanics (Cambridge University Press, Cambridge, England, 1957), p. 420.

[6]D. O. Edwards, A. S. McWilliams, and J. G. Daunt, Phys. Rev. Lett. 9, 195 (1962).

[7]M. F. Panczyk, R. A. Scribner, J. R. Gonano, and E. D. Adams, Phys. Rev. Lett. 21, 594 (1968).

[8]I. Prigogine, R. Bingen, and J. Jeener, Physica 20, 383 (1954); I. Prigogine and J. Jeener, ibid. 20, 516 (1954); I. Prigogine, R. Bingen, and A. Bellemans, ibid. 20, 633 (1954); I. Prigogine, The Molecular Theory of Solutions (North-Holland, Amsterdam, 1957), p. 400.

[9]P. G. Klemens, R. de Bruyn Ouboter, and C. Le Pair, Physica 30, 1863 (1964).

[10]R. A. Coldwell-Horsfall, in Proceedings of the Ninth International Conference on Low Temperature Physics, Columbus, Ohio, 1964, edited by J. G. Daunt, D. O. Edwards, F. J. Milford, and M. Yaqub (Plenum, New York, 1965), p. 1110.

[11]W. J. Mullin, Phys. Rev. Lett. 20, 254 (1968).

[12]M. Uwaha and G. Baym, Physica 107B, 279 (1981).

[13]B. A. Fraass and R. O. Simmons, Physica 107B, 277 (1981).

[14]B. A. Fraass and R. O. Simmons, Phys. Rev. B 36, 97 (1987).

[15]S. Ehrlich, Ph.D. dissertation, University of Illinois, 1986; S. Ehrlich and R. O. Simmons, J. Low Temp. Phys. 68, 125 (1987).

[16]S. Ehrlich and R. O. Simmons, Can. J. Phys. 65, 1569 (1987).

[17]I. Iwasa and H. Suzuki, in Proceedings of the Fourth International Conference on Phonon Scattering in Condensed Matter, Stuttgart, 1983, edited by W. Eisenmenger, K. Lassman, and S. Dottinger (Springer, Berlin, 1984), p. 260. Note that the bulk modulus of a bcc ^{3}He crystal of 24 cm^3 molar volume is taken as 300 atm. in this paper, whereas 183 atm is a more accurate value.

[18]G. C. Straty and E. D. Adams, Phys. Rev. 150, 123 (1966).

[19]E. R. Grilly, J. Low Temp. Phys. 11, 33 (1973).

[20]D. O. Edwards and R. C. Pandorf, Phys. Rev. 144, 143 (1966).

[21]J. K. Hoffer, W. R. Gardner, C. G. Waterfield, and N. E. Phillips, J. Low Temp. Phys. 23, 63 (1976).

[22]D. O. Edwards and R. C. Pandorf, Phys. Rev. A 140, 816 (1965).

[23]W. R. Gardner, J. K. Hoffer, and N. E. Phillips, Phys. Rev. A 7, 1029 (1973).

[24]V. N. Grigoriev, B. N. Eselson, and V. A. Mikheev, Zh. Eksp. Teor. Fiz. 66, 321 (1974) [Sov. Phys.—JETP 39, 153 (1974)].

[25]D. S. Miyoshi, R. M. Cotts, A. S. Greenberg, and R. C. Richardson, Phys. Rev. A 2, 870 (1970).

[26]J. H. Vignos and H. A. Fairbank, Phys. Rev. 147, 185 (1966).

[27]I. Iwasa and H. Suzuki, in Proceedings of the 17th International Conference on Low Temperature Physics (LT 17), Karlsruhe, 1984, edited by V. Eckern, A. Schmid, N. Weber, and H. Wuhl (North Holland, Amsterdam, 1984).

[28]R. H. Arnold and P. B. Pipes, Phys. Rev. 21, 5156 (1980).

[29]P. N. Henrickson, M. F. Panczyk, and E. D. Adams, Solid State Commun. 8, 735 (1970); S. B. Trickey, W. P. Kirk, and E. D. Adams, Rev. Mod. Phys. 44, 668 (1972).

[30]A. S. Greenberg, W. C. Thomlinson, and R. C. Richardson, J. Low Temp. Phys. 8, 3 (1972).

[31]A. E. Burgess and M. J. Crooks, Phys. Lett. 39A, 183 (1972).

[32]V. N. Zharkov and V. P. Silin, Zh. Eksp. Teor. Fiz. 37, 143 (1960) [Sov. Phys.—JETP 10, 102 (1960)].

[33]J. P. Laheurte, J. Low Temp. Phys. 12, 127 (1973).

[34]D. S. Greywall and P. A. Busch, J. Low Temp. Phys. 46, 451 (1982).

[35]E. R. Grilly, J. Low Temp. Phys. 4, 615 (1971).

[36]R. A. Scribner, M. E. Panczyk, and E. D. Adams, J. Low Temp. Phys. 1, 313 (1969).

[37]W. P. Halperin, F. B. Rasmussen, C. N. Archie, and R. C. Richardson, J. Low Temp. Phys. 31, 617 (1978).

[38]C. Ebner and D. O. Edwards, Phys. Rep. 2C, 77 (1970).

[39]G. E. Watson, J. D. Reppy, and R. C. Richardson, Phys. Rev. 188, 384 (1969).

[40]B. M. Abraham, Y. Eckstein, J. B. Ketterson, M. Kuchnir, and P. R. Roach, Phys. Rev. A 1, 250 (1970).

[41]J. Landau, J. T. Tough, N. R. Brubaker, and D. O. Edwards, Phys. Rev. A 2, 2472 (1970).

[42]J. R. Owers-Bradley, R. M. Bowley, and P. C. Main, J. Low Temp. Phys. 60, 243 (1985).

[43]R. M. Bowley, J. Low Temp. Phys. 61, 291 (1985).

[44]A. Ghozlan and E. Varoquaux, Ann. Phys. (Paris) 4, 239 (1979).

[45]V. N. Lopatik, Zh. Eksp. Teor. Fiz. 86, 487 (1984) [Sov. Phys.—JETP 59, 284 (1984)].

[46]B. Hebral, A. S. Greenberg, M. T. Beal-Monod, M. Papoular, G. Frossati, H. Godfrin, and D. Thoulouze, Phys. Rev. Lett. 46, 42 (1981); B. Castaing, A. S. Greenberg, and M. Papoular, J. Low Temp. Phys. 47, 191 (1982).

[47]B. van den Brandt, W. Griffioen, G. Frossati, H. van Beelen, and R. de Bruyn Ouboter, Physica 114B, 295 (1982).

[48]K. N. Zinovieva, Zh. Eksp. Teor. Fiz. 44, 1837 (1963) [Sov. Phys.—JETP 17, 1235 (1963)].

[49]L. D. Landau and E. M. Lifshitz, Statistical Physics (Pergamon, New York, 1960), p. 310.

[50]H. Weinstock, F. P. Lipschultz, C. F. Kellers, P. M. Tedrow, and D. M. Lee, Phys. Rev. Lett. 9, 193 (1962).

[51]I. M. Lifshitz and D. G. Sanikidze, Zh. Eksp. Teor. Fiz. 35, 1020 (1958) [Sov. Phys.—JETP 35, 713 (1959)].

[52]V. A. Mikheev, V. A. Maidanov, and N. P. Mikhin, Fiz. Nizk. Temp. 12, 658 (1986) [Sov. J. Low Temp. Phys. 12, 375 (1986)].

[53]P. H. Bevington, Data Reduction and Error Analysis for the Physical Sciences (McGraw-Hill, New York, 1969), p. 237.